Th P9 15

Imaging of Sumatra Gas-rich Region Using 2D Hierarchical Viscoelastic Waveform Inversion

T. Belahi (Institut de Physique du Globe de Paris), N. Fuji* (Institut de Physique du Globe de Paris), S. Singh (Institut de Physique du Globe de Paris)

Summary

We present a hierarchical strategy of viscoelastic full waveform inversion and its application to a real dataset.We show first that, in synthetic tests, mid-offset and far-offset data are particularly sensitive to attenuation and thus purely elastic waveform inversion can fail to obtain a meaningful model, i.e. simultaneous inversion of both elastic and anelastic parameters is required in order to properly treat reflections and converted waves close to the critical angle. We then apply our viscoelastic inversion scheme to long-offset (15 km) data acquired offshore Sumatra. A previous study using (purely) elastic full waveform inversion using the same data on the Mentawai forearc basin dataset found a low velocity anomaly, which could possibly be interpreted as a gas pocket. We apply, rather, our viscoelastic full waveform inversion strategy to the long offset data. We inverted using refracted waves in combination with a frequency continuation approach. In the later stage of the frequency continuation strategy, we included long-offset reflection data that granted access to the smaller wavelength of the model. We inverted simultaneously for elasticity and anelasticity at every stage of the inversion. The final resolution of the velocity model is increased and the dipping structures are better imaged.

Introduction

Waveform inversion has become a standard tool in exploration geophysics but there are still many limitations not only in terms of computational costs but also in parameterisation. The acoustic and/or elastic waveform inversions have shown their successfulness in various geological settings but could fail to properly image the Earth's subsurface in the presence of high attenuation, such as gas clouds, hydrate bearing sediments or unconsolidated sediments, which is not considered in the classical acoustic/elastic inversions. It seems reasonable, for the first place, to take into account anelastic parameters during forward modelling within classical inversion scheme for purely (acoustic) parameters (e.g. Kurzman et al. 2013) but it turns out that simultaneous inversions for both elasticity and anelasticity are needed to constrain acoustic/elastic features of mid- or short-wavelengths (e.g. Belahi et al. 2015; 2016). However, it is not trivial to extract meaningful information on attenuation from seismic data since the sensitivity for elasticity and anelasticity are essentially coupled (e.g. Fuji et al. 2010) and it is essential to design hierarchical inversion in order not to misinterpret the seismic signals. In this paper, we first present our strategy of hierarchical viscoelastic waveform inversion based on synthetic tests on a Marmousi-2 model (Martin et al. 2002) then its application to an ultra-long offset data acquired offshore Sumatra, comparing its results with that obtained using purely elastic inversion.

Method

We use classical full waveform inversion with a least square of waveform difference between observed and synthetic as a cost function to minimise, by iteratively computing the gradient direction of the misfit (Lailly, 1983; Tarantola 1984). In order to take into account viscoelasticity, we use one Standard Linear Solid (SLS) assumption to parameterise the stiffness tensor, yielding a simplified time-dependent Hooke's law:

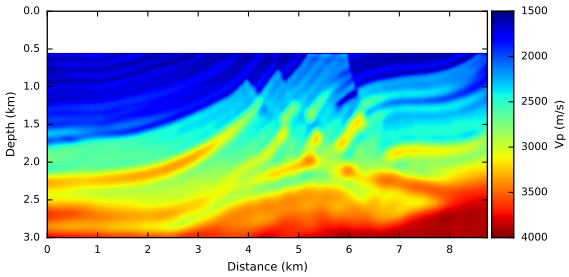
$$\sigma^{ij}(\mathbf{x},t) = \Psi^{ijkl}(\mathbf{x},0^+)\varepsilon^{kl}(\mathbf{x},t) + \Delta\Psi^{ijkl}(\mathbf{x})\epsilon^{kl}(\mathbf{x},t) \tag{1}$$

with σ^{ij} the stress, ε^{ij} strain, $\Psi^{ijkl}(\mathbf{x},0^+)$ initial stiffness matrix, $\Delta\Psi^{ijkl}(\mathbf{x})$ the difference of stiffness matrix at time ∞ and the initial time, ϵ^{ij} the memory strain variables that account for the energy dissipation (e.g. Robertsson et al. 1994). When we assume an isotropic medium, Ψ^{ijkl} will have two independent Lamé's parameters, resulting in inversion for four independent parameters $\lambda(\mathbf{x},0^+)$, $\mu(\mathbf{x},0^+)$, $\Delta\lambda(\mathbf{x})$, $\Delta\mu(\mathbf{x})$ that can then be mapped into V_p, V_s, Q_p and Q_s (e.g. Tarantola 1988; Belahi et al. 2016). As we show in the synthetic experiment using Marmousi-2 model, simultaneous inversions for elasticity and anelasticity are important to recover a clear seismic image in the presence of attenuation.

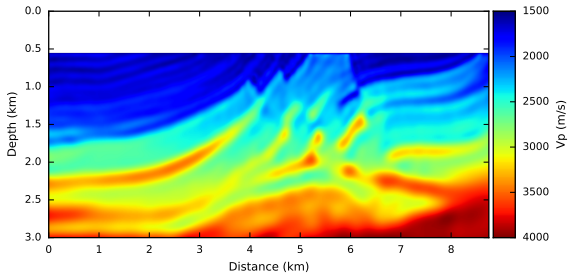
Synthetic tests

In order to assess the importance of simultaneous inversion, we used a modified Marmousi-2 model with Q_p and Q_s correlated to V_p and V_s , ranging from 20 to 150 and 10 to 120, respectively. The Marmousi model with its steep dips and the strong velocity variations is challenging to image and makes a suitable benchmark for waveform inversion. We generate 62 shots, with 7.5 Hz Ricker wavelet source time function, with 125 m spacing and 351 receivers spaced by 25 m on the sea bottom. We run two experiments: i) "active" inversions for all four parameters V_p,V_s,Q_p and Q_s; and ii) "passive" inversions only for V_p and V_s, which, yet, takes into account viscoelasticity in forward modelling. Since the second method, by its nature, yields seismic images superior to that with the aid of the first method, we deliberately show results using Limited-Memory BFGS algorithm (e.g. Liu & Nocedal 1989) for the first experiment, whereas we show results using only conjugate gradient algorithm for the latter. For both experiments, we first performed 40 iterations for lower frequency band (0-3.5 Hz) and included higher frequencies (0-5.5 Hz) for later 40 iterations. We show final V_p and V_s images in Fig. 1. In order to objectively evaluate the quality of these images, we define ℓ_1 norm of Model Distance Reduction "MDR" as MDR $= \left[1 - ||\mathbf{m}^{\text{inv}} - \mathbf{m}^{\text{start}}||/||\mathbf{m}^{\text{true}} - \mathbf{m}^{\text{start}}||\right]$ (%).

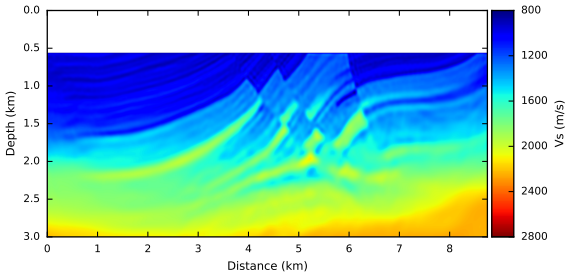
(a) Final V_p model (active inversion)



(b) Final V_p model (passive inversion)



(c) Final V_s model (active inverison)



(d) Final V_s model (passive inversion)

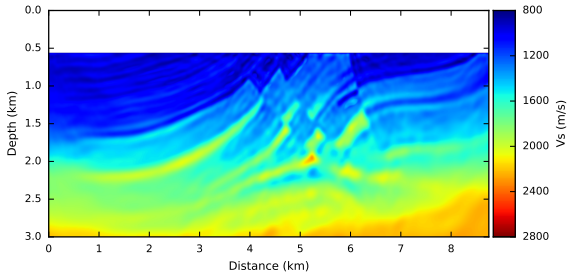


Figure 1: Final models V_p and V_p models for "active" and "passive" inversions.

MDR (in %)	Vp (0-3.5 Hz)	Vs (0-3.5 Hz)	Vp (0-5.5 Hz)	Vs (0-5.5 Hz)
active above 1.5 km	51	57	62	66
active below 1.5 km	12	10	19	17
passive above 1.5 km	47	51	54	49
passive below 1.5 km	16	15	20	19

Table 1: MDR (model distance reduction) for active and passive inversions: bigger numbers (coloured in red when there is >5 % of difference) show the superiority to the opponent method.

We show in Table 1 the MDR values for all the inversions including the intermediate results after 40 lower frequency iterations. Note that we evaluate MDR independently for shallow and deep part with a border at 1.5 km depth. We observe that L-BFGS passive method can slightly be more accurate for deeper part due to its better conditioning of inverse Hessian, whereas shallower part shows always better MDR with active inversions even with a simple conjugate gradient. However, for deeper part, simultaneous active inversions yield seismic images of the same order of quality, when we gradually include the higher frequencies, mid- and far- offset reflection events become dominant signals, which are particularly sensitive to attenuation. Due to the difference of sensitivity of reflection and refraction data to elasticity and anelasticity, we propose hierarchical inversions in terms of frequency bands and events. Even though the resulting Q models (not shown here) are not fully accurate, simultaneous inversion helps to unlock the mapping of higher-wavelength data in the velocity models, enabling the inversion to yield sharper and better resolved velocity models.

Real data inversion

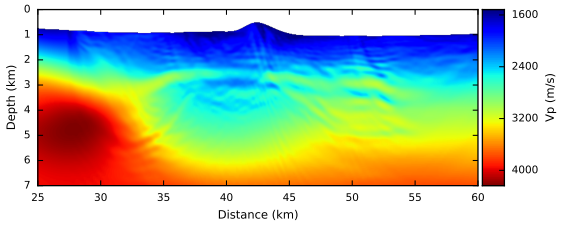
The Sumatra subduction zone is the plate boundary between the the Indo-Australian plates and the Sunda plate. There have been several great earthquakes since 2004. In order to understand the nature of this region, an active experiment of with 15 km-long streamer was conducted with

CGGVeritas' Geowave Champion seismic vessel in 2009. We have shot spacing of 50 m and receiver spacing of 12.5 m. Huot & Singh (2015) applied traveltime tomography and elastic waveform inversion only for V_P by linking V_S and ρ to V_P by a simple relationship (Gardner et al. 1974), finding a low velocity zone that may indicate the presence of fluid or gas. In this study, we focus on the centre of the forearc basin where we used 444 shots. Data are preprocessed to remove various noises.

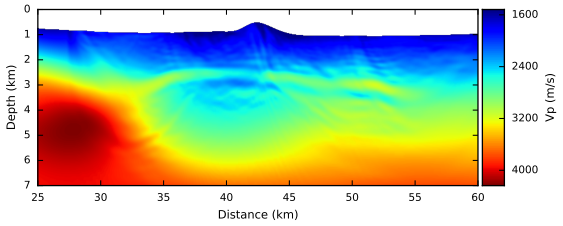
Prior to waveform inversions, we performed travel time tomography to obtain a proper initial model. We first invert the refraction only for 1-6 Hz with 25 iterations then for 1-9 Hz with 25 iterations in order to improve the long-wavelength features. We finally jointly invert for refracted and reflected data for 1-12 Hz with 25 iterations. We conducted simultaneous and purely elastic inversions. Final V_p and Q_p images are shown in Fig. 2. We also show here purely elastic results from Huot& Singh (2015) that used also gradually increasing frequency bands but always invert both for refraction and reflection. The improved structure obtained with our (visco)elastic inversion strategy suggest that when inverting jointly different types of seismic events, they may have conflicting effects or lead to a local minimum in the misfit function. Event separation in hierarchical way serves as a crude form of data regularisation.

The comparison between the viscoelastic V_p model (Figure 2a) and the elastic V_p model (Figure 2b) highlights that the use of the viscoelastic full waveform inversion scheme yielded a model that has a higher resolution and also a better lateral continuity. However, the improvement of the V_p model is not uniform over the whole model space, the main differences and improvement lie in the forearc basin, at the distances between 47 and 55 km, especially when it comes to dipping reflectors that are much more visible in the viscoelastic model. The improvement of the model are less important around the low velocity zone and west of it, between the distances 30 and 47 km. This means that the improvement brought by viscoelastic full waveform inversion in the area of high reflectivity as compared to the area of lower reflectivity identified on the PSTM image.

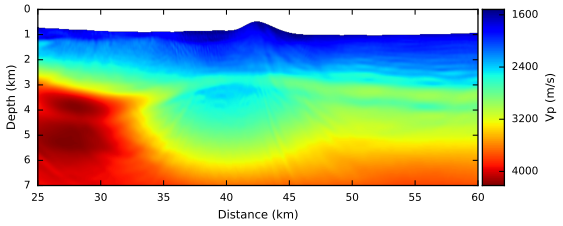
(a) Viscoelastic P-wave velocity



(b) Elastic P-wave velocity



(c) Elastic P-wave velocity without hierarchy



(d) Q_p model

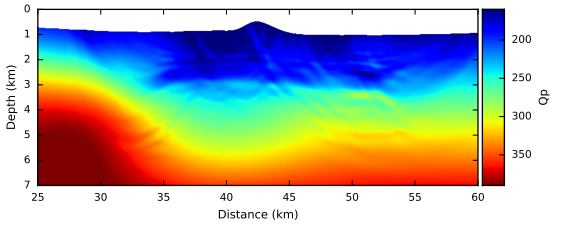


Figure 2: V_p models obtained by three different strategies and Q_p final model by viscoelastic approach.

Discussion

Our inversions confirmed the presence of a low velocity zone below the push-up ridge, it is clearly visible at around 3 km depth (Figure 2a). This low velocity zone is not correlated

with low quality factor zone of similar shape (Figure 2d). Therefore, our results do not point clearly to the presence of gas or to the characterisation of any fluid. However, the cap rock in Figure 2a is not as continuous as in Figure 2c and this may indicate a connection between the low velocity and the overburden. There are two noticeable geological features that can be observed there. First, a flat reflector is revealed at around 5 km depth at the distances greater than 47 km. Second, we see an area of low velocity located at 2.5 km that is not visible in the elastic inversion results. It matches a patch of low quality factor in our final results (Figure 2d). This may indicates the presence of gas. This feature is located at the edge of our model and would require that we include more shots to be properly constrained.

Conclusions

We have successfully applied viscoelastic full waveform inversion to ultra-long offset from offshore Sumatra. The presence of broadband and long offset reflection data has allowed the inversion both elasticity and anelasticity. The inclusion of attenuation in the inversion increases the resolution of P-wave velocity model as the waveforms are properly corrected. Our results confirm that the attenuation is most sensitive to critical and post-critical reflection data as predicted by analytical experiments (e.g. Belahi et al. 2015).

Acknowledgements

The research described in this abstract was carried out as a part of the Paris Exploration Geophysics group project (GPX) funded by the French National Research Agency (ANR), CGG, Schlumberger and Total. Numerical computation were performed on the S-CAPAD platform at IPGP.

References

Belahi, T., Fuji, N., Singh, S. C. [2015] Elastic Versus Viscoelastic Full Waveform Inversion of Near-offset and Wide-angle Data in the Presence of Attenuation. *77th EAGE Conference and Exhibition 2015*, pp. 1-4

Belahi, T., Singh, S.C., Fuji, N. [2016] Viscoelastic full waveform inversion of sea bottom long offset seismic data in presence of attenuation, *78th EAGE Conference and Exhibition 2016*, pp.1-4

Huot, G., Singh, S.C. [2015] Imaging of a large amount of free gas in Sumatra forearc basin using elastic full waveform inversion. *77th EAGE Conference and Exhibition 2015*, pp. 1-4

Kurzmann, A., Przebindowska, A., Kohn, D., Bohlen, T. [2013] Acoustic full waveform tomography in the presence of attenuation: a sensitivity analysis. *Geophys. J. Int.,* 195(2), pp. 985-1000

Fuji, N., Kawai, K., Geller, R.J. [2010] A methodology for inversion of broadband seismic waveforms for elastic and anelastic structure and its application to the mantle transition zone beneath the Northwestern Pacific. *Phys. Earth Planet. Inter.*, 180, pp. 118-137.

Lailly, P. [1983] The seismic inverse problem as a sequence of before stack migration. *Conference on Inverse Scattering, Theory and Applications, SIAM, Expanded Abstracts*, 206-220

Liu, D.C., Nocedal, J. [1989] On the limited memory BFGS method for large scale optimization, *Mathematical Programming*, 45, pp. 503-528.

Martin, G. S., Marfurt, K. J., Larsen, S. [2002] Marmousi-2: An updated model for the investigation of AVO in structurally complex areas. *SEG Technical Program Expanded Abstracts*, 21(1), 1979-1982.

Quintal, B., Steeb, H., Frehner, M., Schmalholz, S. M., Saenger, E. H. [2012] Pore fluid effects on S-wave attenuation caused by wave-induced fluid flow. *Geophysics*, 77(3), L13-L23

Robertsson, J. O., Blanch, J. O., Symes, W. W. [1994] Viscoelastic finite-difference modeling. *Geophysics*, 59(9)

Tarantola, A. [1988] Theoretical Background for the Inversion of Seismic Waveforms, Including Elasticity and Attenuation. *Pure and Applied Geophysics*, 128, pp. 365-399